Revisiting the demagnetization curves of Dy-diffused Nd-Fe-B sintered magnets

J. Fliegans, C. Rado, R. Soulas, L. Guetaz, O. Tosoni, Nora Dempsey, G. Delette

Revisiting the demagnetization curves of Dy-diffused Nd-Fe-B sintered magnets

J. Fliegans[1,2], C. Rado[1], R. Soulas[1], L. Guetaz[1], O. Tosoni[1], N.M. Dempsey[2], G. Delette[1,a)]

[1]Univ. Grenoble Alpes, CEA, LITEN, DTNM, 38000 Grenoble, France

[2]Univ. Grenoble Alpes, CNRS, Grenoble INP, Institut Néel, 38000 Grenoble, France

[a)]Author to whom correspondence should be addressed: gerard.delette@cea.fr

Abstract

The grain boundary diffusion process (GBDP) is now widely used to increase coercivity in Nd-Fe-B sintered magnets with a more efficient use of heavy rare earth elements (Dy, Tb). This process leads to a typical core-shell structure for the grains consisting of $(Nd,Dy)_2Fe_{14}B$ shells at the outer grain regions and $Nd_2Fe_{14}B$ cores. The thickness of the $(Nd,Dy)_2Fe_{14}B$ shells decreases from the diffusion surface to the magnet core. This inhomogeneous distribution in Dy content gives rise to a coercivity gradient within the magnet and leads therefore to a reduced squareness of the demagnetization curve. The purpose of this work is to provide a quantitative understanding of the influence of composition profiles after GBDP on the shape of the demagnetization curve of Nd-Fe-B sintered magnets diffused with the $Dy_{63}Co_{37}$ (at. %) intermetallic compound. SEM/X-EDS analyses along the Fisher diffusion model allow the estimation of the Dy concentration in grains and at different depths. Then, after ascribing to the grains some critical values for the switching field that are related to the local Dy content, a macroscopic finite element model is implemented to provide a better understanding of the grain reversal sequence in the graded magnets tested in closed-circuit. Grain reversal patterns show that demagnetization starts from the less coercive grains in the magnet core, remains constricted in this zone thanks to a shielding effect from the external surface, and then propagates towards outer layers via magnetostatic interactions. When the coercivity gradient is large, the coercivity of the whole magnet measured in closed-circuit could be 100-200 kA/m lower than the value expected without considering magnetostatic interactions, suggesting that the shielding effect from the diffusion affected layers could be limited and counterbalanced by magnetostatic interactions.

Keywords: Nd-Fe-B, grain boundary diffusion process, coercivity, magnetostatic interactions

1. Introduction

The coercivity of sintered Nd-Fe-B magnets is strongly correlated with the local magnetic properties in the vicinity of grain boundaries where high demagnetizing fields and degradation of the anisotropy field favour the nucleation of reversed domains. Partial substitution of Dy for Nd in the hard magnetic phase (up to 8-10 % for motor applications) has traditionally been employed to compensate these detrimental effects with the higher intrinsic anisotropy field of $(Nd_x,Dy_{1-x})_2Fe_{14}B$ compounds [1]. The Grain Boundary Diffusion Process (GBDP) [2] is now widely used to increase coercivity with a more efficient use of the Heavy Rare Earth Elements (HREEs). During this thermal treatment, the HREE (Dy, Tb) penetrates into the bulk of the magnet from a surface coating applied after sintering. Penetration occurs preferentially along grain boundaries, owing to the formation of an intergranular liquid phase around 900°C. This process leads to HREE enrichment of the outer shell of the grain while the composition of the grain interior remains almost unchanged. The resulting core-shell structure exhibits different characteristics along the direction of penetration: the thickness of the shell is typically about 1 μm at a depth of 50-100 μm beneath the surface of the magnet and decreases to 10 nm at a depth of 0.5-1 mm [3]. The distribution in HREE content inevitably leads to a coercivity gradient within the magnet, the central inner region being less resistant to demagnetization than the outer region. Such a heterogeneity in magnetic properties accounts for a reduced squareness in the hysteresis curve of the magnet, which is detrimental for applications. Moreover, it is not clear for system designers if the outer region of such a grain-boundary diffused magnet can efficiently shield the overall magnet from demagnetization during operation.

This work aims at providing a quantitative understanding of the influence of composition profiles after GBDP on the shape of the demagnetization curve of a magnet. A numerical simulation of the magnetostatic field considering a large population of magnetized grains, which is representative of sintered hard magnets working in closed-circuit, is implemented to investigate how grain reversal patterns develop in such polycrystalline graded magnets.

2. Experimental and numerical methods

2.1 Sample preparation and characterization

Sintered magnets of composition $(Nd,Pr,Dy)_{31}Fe_{67.1}B_1Al_{0.3}Co_{0.5}Cu_{0.1}$ (wt.%), with a low overall Dy content of 0.5 wt.% were used as base magnets. The samples have been manufactured by the conventional powder metallurgy route involving alloy synthesis by strip-casting followed by pulverization of the produced ribbons by hydrogen decrepitation and jet-milling, leading to a powder with a median diameter of 5 μm. The powder was aligned under a pulsed magnetic field (7 T) and isostatically compacted at 150 MPa. Sintering was performed under vacuum at 1030°C for 4h followed by annealing at 530°C for 2h. The RE excess allows the formation of a Nd-rich phase at grain boundaries, which favours densification and enhances coercivity by decoupling neighbouring grains which are, after annealing, separated by a continuous non-ferromagnetic phase containing most of the additional elements (Al, Cu) [4] .

The magnetic properties of magnets were measured in the closed-circuit configuration (hysteresigraph AMH-300-P from Laboratorio Elettrofisico) after machining into regular cylinders. The remanent induction of the sintered magnet after annealing was found to be 1.36 T and the coercivity equal to 1086 kA/m. A three axis magnetic field scanner based on Hall probes (SENIS Magnetic Field Mapper), was used to measure the residual magnetic field produced above the top of the magnets. The distance from the sensor to the magnet surface was 400 μm and the displacement step was 100 μm. This equipment allowed magnetization patterns to be mapped after partial demagnetization and revealed details at the sample surface with a spatial resolution of about 100-400 μm.

The sintered magnets were submitted to GBDP using the intermetallic compound $Dy_{63}Co_{37}$ that exhibits congruent melting at T_M=734°C. This alloy was prepared by melting Dy and Co at 850°C for 20 minutes. In a glove box, the ingot was then crushed into flakes and further ground in a mortar to obtain a powder with an average particle size of about 50 μm. The diffused Nd-Fe-B sintered magnets are cylindrical, with a thickness of about 5 mm and a diameter of about 10 mm. Before diffusion experiments, the magnets underwent chemical cleaning in a dilute nitric acid solution to remove surface oxidation layers. The diffusion source used for GBDP is an ink fabricated by mixing the Dy-Co powder with Terpineol. Mixing was performed so that the ink was composed of about 65 wt.% of Dy-Co powder, for optimal viscosity. The ink with 20 mg of $Dy_{63}Co_{37}$ was then coated onto the top and bottom surfaces of the magnets, which are perpendicular to the

easy-axis (revolution axis), so that the magnet was diffused symmetrically with a limited amount of 0.8 wt.% of Dy. The diffusion heat treatment was performed in a vacuum furnace under three different conditions: 870°C for 3h and 920°C for 3 and 12h. For microstructural characterization, the magnets were embedded and polished. Scanning electron microscopy (SEM) investigations were carried out using a Zeiss MERLIN Gemini microscope equipped with two Bruker SDD energy-dispersive X-ray spectroscopy (X-EDS) detectors. X-EDS elemental maps were acquired at 5 kV in different areas located along the axis of the magnets. Semi-quantitative analysis of the alloy chemical composition were extracted from the maps in order to draw a representative Dy concentration profile across grain boundaries using the classical phi-rau-z method of the X-EDS software.

Magnetic properties were measured on the magnet annealed at 920°C for 3h, both before and after removing, in a symmetrical manner, thin layers from the top and bottom surfaces of the magnet. This approach allows analyzing the magnetic property gradient and enables a correlation with the microstructural gradient revealed by X-EDS analysis.

2.2 Demagnetization simulation of polycrystalline magnets

Micrometric grains in Nd-Fe-B sintered hard magnets are widely considered as being exchange-decoupled [5]. In contrast with soft ferromagnetic materials, magnetization reversal in such a granular medium can be seen as a discrete process growing by elementary steps, which reflects the switching of individual grains [6].

In the following simulation, the polycrystalline hard magnet is depicted as a regular array of identical cubic grains. Each grain is assumed to be homogeneously polarized along the axial direction and its magnetization can switch abruptly, when the field exceeds a given threshold, from the initial positive value $+J_S$ to the negative value $-J_S$ without any angular deviation from the easy axis. The combination of non-reversed and reversed grains upon demagnetization leads to a non-trivial distribution of the magnetic field. Moreover, the local magnetic field depends also on the external structure that, in most practical cases, surrounds the magnet. This particular configuration creates a coupling between the macroscopic environment and the local grain environment.

This magnetostatic problem is solved here by a finite element (FE) commercial software (Flux 3D, Altair) monitored by a specific Python script. Each grain is meshed with 64 quadratic cubic elements refined near the edges and corners. In order to reduce the model

size, three symmetry planes (x=0, y=0 and z=0) are considered, allowing only 1/8 of the total volume to be actually simulated [7].

The Flux 3D code was used to solve the partial differential equations system for standard magnetostatic problems in which the polarization J and the magnetic field H are the unknowns. The problem was solved assuming the magnet is located in the gap of a magnetic circuit that applies an external field to the magnet via winding coils, a yoke and pole pieces (see Fig. 1). This model represents the main features of the hysteresigraph equipment employed for making magnetic measurements. This configuration is denoted closed-*circuit* and the magnetic circuit suppresses the magnet's self-demagnetizing contribution to the applied field. The non-linear magnetic behaviour of the ferromagnetic pole pieces has a negligible effect on the results.

Magnetization reversal is triggered in a given grain when the projection of the local magnetic field H value along the z-axis, averaged on the grain volume, exceeds the critical field H_C assigned to the grain. A Gaussian distribution of the switching field is ascribed to the grain population to reflect the inherent variation of grain size and defects in real materials. The mean value $\langle H_C \rangle$ and the standard deviation σ_{Hc} are input parameters of the model and will be further discussed below. At the beginning of the simulation, all the grains are polarized along the +z direction yielding the remanent state reached after saturation. An external magnetic field is then applied to the magnetic in the opposite direction, and its intensity is progressively increased by small increments ΔH. For each increment, the reversal condition is tested on all grains and, when fulfilled, the polarization of the grains is switched. Since each grain reversal changes the overall magnetostatic field, the test is repeated in a sub-iterative loop until a stable magnetization pattern is achieved. Then, the next step with a new field increment is performed considering the previously updated grain magnetization pattern as an input for calculating the new local magnetic field.

The polycrystalline model should be seen as a very simplified representation of sintered magnets. First, the spatial discretization of the cubic grains is not fine enough to capture the demagnetizing field details near grain boundaries, at the scale at which nucleation occurs [8]. The switching field of grains is therefore considered as input data, disregarding details such as local orientation effects, considered in the Stoner-Wohlfarth model. The second model limitation stems from the number of grains that can be simulated (up to 4000). However, in this approach, the grain size is not really a relevant factor since dipolar

effects are averaged over the grain volume, making the results identical whatever the cube size. Consequently, macroscopic magnets are simulated by 3D arrays of arbitrary sized grains, the aspect ratio of the array being the same as the magnet. This allows the demagnetizing field to be correctly described at both magnet and grain scale. Obviously, the weight of a cubic grain reversal in the simulation is considerably higher than that of a real grain, resulting in highly stepped J-H curves.

2.3 Calculation of Dy concentration after diffusion annealing

Dy penetration in sintered magnets results from a combination of grain boundary and volume diffusion mechanisms. An early model introduced by Fisher [9] considers a 2D bi-crystal with two semi-infinite planar domains separated by a thin vertical layer (x=0, accounting for the grain boundary) taken as being perpendicular to the top line (y=0) where the diffusing species are initially deposited. Diffusion kinetics are assumed to follow Fick's law in each medium (low diffusivity D_v in grains and high diffusivity D_j along grain boundaries (GB). At the initial state, the concentration of HREE is assigned to be equal to 1 at the top line (y=0) and is zero in the volume. Fisher obtained the following analytical expression for the concentration profile:

$$c(\xi,\eta,\beta) = erfc\left(\frac{\xi}{2}\right) \times exp\left(-\frac{\eta}{\pi^{1/4}\beta^{1/2}}\right) \quad \text{[Eq. 1]}$$

The reduced coordinates are expressed as (with a being the half width of the grain boundary):

$$\xi = \frac{x-a}{\sqrt{D_v t}} \qquad \eta = \frac{y}{\sqrt{D_v t}} \qquad \beta = \frac{D_j}{D_v}\frac{a}{\sqrt{D_v t}}$$

The concentration given in [Eq. 1] is a product of two distinct terms. The first one (error function) depicts the lateral profile in grains with respect to the x-coordinate and represents therefore the consumption of the diffusing species by the grains. The second term takes into account diffusion along the grain boundary (i.e. along the y-axis). The attenuation of the penetration profile is described with an exponential function (i.e. the factor β). When the factor β is small, the iso-concentration lines tend to be flat, diffusion being controlled by volume diffusion and limited to a thin layer under the sample surface. On the contrary, when the factor β is high, diffusion along GBs is predominant and the iso-concentration lines become very steep (sharp) near GBs. This is the case in the current diffusion annealing conditions, for 920°C/3h the value of β being estimated to be equal to 4.10^5.

The Fisher approximation holds when the concentration profile remains flat along the thickness of the grain boundary (along the x-axis) and for an infinite source of Dy available at the sample surface. Whipple [10] improved the model for large GBs (non-flat profile) and Suzuoka [11] proposed a solution taking into account the consumption of the diffused element. However, these last two formalisms are more complicated and the solutions require numerical evaluation. As a first approach, the Fisher approximation has been implemented in this study in order to establish some main trends.

Diffusion annealing was carried out within a range of temperature for which a liquid phase forms at GBs via the eutectic reaction between the Nd-rich phases localized at GBs and the $Nd_2Fe_{14}B$ grains. The eutectic reaction occurs at 677°C [12,13] and the resulting liquid phase tends to wet the GBs before the onset of melting of the $Dy_{63}Co_{37}$ alloy (734°C). The values of diffusion coefficients D_v and D_j are the key parameters in this model and should reflect the preferential diffusion in the GB liquid phase. For the volume diffusion of Dy in $Nd_2Fe_{14}B$ grains, the following expression proposed by Campos et al. [14] for the coefficient D_v has been considered:

$$D_v[m^2.s^{-1}] = 8.10^{-4} exp\left(-\frac{315\,000}{R.T[K]}\right) \qquad \text{[Eq. 2]}$$

The diffusion coefficient D_j has been evaluated by Loewe *et al.* [15] for some rare-earth elements (Dy, Tb) at 900°C from coercivity profiles ($D_j = 1.1\ 10^{-10}\ m^2.s^{-1}$, *i.e.* $D_j/D_v \approx 10^7$). For other temperatures, it has been assumed that the value of D_j evolves from the "pivot" temperature of 900°C, according to an Arrhenius law, with an activation energy Q_j of 315 kJ/mol, equivalent to bulk diffusion. The exact activation energy is unknown but the following trends are not drastically changed for other values of Q_j, due to the narrow range of temperature studied (50 °C).

It should be noted that the width of the grain boundary has been taken as $2a$=20 nm, which is larger than that observed by TEM analysis at room temperature [16]. Since the grain surfaces are partially melted at 900°C, a larger value for the grain boundary thickness can be reasonably assumed during the diffusion heat treatment. This value also corresponds to an estimation made from the STEM-EDX lines measured on GBs by Loewe *et al.* [15].

2.4 Grain switching field as a function of the local Dy concentration

As mentioned before, a critical value for the switching field is ascribed to each grain of the polycrystalline model in order to simulate demagnetization of the graded magnets. For the homogeneous base magnet (before Dy diffusion annealing) the values of the mean grain critical field, $<H_c>$ = 1273 kA/m (1.6 T), and the standard deviation, σ_{Hc}= 160 kA/m (0.2 T), have been selected in such a way that the simulated J-H curve in closed-circuit fits the experimental demagnetization curve (not represented). It has to be pointed out that the value of $<H_c>$ is higher than the experimental coercivity of the base magnet (1086 kA/m), the difference being of the order of the standard deviation. This comes from the fact that when grains with lowest coercivity reverse, they trigger the propagation of switching towards neighbouring grains, due to the proximity of the opposite demagnetising field.

After diffusion annealing, the switching field of grains increases in accordance with the local Dy concentration near GBs. Loewe *et al.* [3] observed core shell structures by SEM/X-EDS and found, by localised magnetic measurements, that the coercivity is locally enhanced as a function of the Dy concentration profile. The coercivity is increased by 250 kA/m (≈0.31 T) in a region located 100 µm beneath the surface: in this region, grains exhibit a Dy-rich shell in which the initial Dy/Nd_{init} ratio, (averaged over 1-µm-depth) is equal to 0.12. Nd_{init} here denotes the atomic content of Nd in the $Nd_2Fe_{14}B$ phase before diffusion and it is used here since Dy substitutes Nd in the diffused region and excess Nd atoms are rejected to GBs [16]. The core-shell structures are no more detectable by SEM/X-EDS analyses at a depth larger than 800 µm, as reported in [3]. Considering that the Dy enrichment is effective only up to 800 µm, this would tend to minimize the actual depth of the magnet over which coercivity is enhanced. Actually, several authors [3,15] observed a local coercivity enhancement up to 2.5-3 mm from the surface in diffused samples, *i.e.* at a distance from the surface for which the Dy enrichment is not revealed by SEM/X-EDS that could be due to the chemical sensibility and spatial resolution limits. However, using STEM-EDX analysis, Loewe *et al.* [3] reported a local Dy concentration of 0.4 at.% at 10 nm from GBs located at 1.5 mm from the magnet surface. This corresponds to an atomic ratio, Dy/Nd_{init}, equal to 0.03. With this low Dy content, the reported coercivity enhancement is still significant (150 kA/m ≈ 0.19 T).

From this data, it has been assumed here that the threshold for grain coercivity enhancement corresponds to a minimum penetration of 10 nm in the grain with a ratio

$Dy/Nd_{init} \approx 0.01$. Finally, the simulation of graded magnets was performed according to the following scheme:

1. The 3D array of grains is sized to the actual magnet dimensions ($10 \times 10 \times 5$ mm) and divided into 2D layers of cubic elements stacked from the center to the surface. In each layer, the Dy concentration is assumed to be homogeneous.
2. For each layer, the lateral Dy concentration depletion from the grain boundary is analytically calculated with the Fisher model, taking into account the distance from the surface, the temperature and the duration of annealing.
3. The average value of the ratio Dy/Nd_{init} (over a shell of 1µm wide) is calculated and the local coercivity enhancement is proportionally ascribed to the grain at a rate of 250 kA/m for a Dy/Nd_{init} ratio of 0.12 (*i.e.* 21 kA/m per 1% Dy/Nd_{init}).
4. The Dy/Nd_{init} ratio is also averaged over a shell width of 10 nm and a minimal coercivity enhancement of 150 kA/m is applied to the grain if $Dy/Nd_{init} > 0.01$.
5. As input for the FE magnetostatic simulation a switching field value is ascribed to each grain. A Gaussian distribution centered on the previous values of coercivity, deduced from the Dy concentration, is used.

It is worth noting that the objective of this approach was not to obtain an accurate determination of the coercivity gradient in magnets. The aim is rather to use the simulation to investigate the influence of such a property gradient, estimated with some reasonable assumptions. The results would undoubtedly be improved with direct measurements of local changes in coercivity.

3. Results

3.1 Diffusion profiles

The lateral Dy concentration profiles (along the x-axis) obtained with the Fisher model account for the Dy penetration into grains. The profiles were calculated for different depths from the magnet surface (100, 200, 400 and 800 µm) for the three experimental diffusion conditions used here (920°C-3h, 920°C-12h and 870°C-3h). From these curves, the values of the Dy concentration, averaged over a shell of width 1 µm located at the grain rim, have been calculated and reported in Table 1.

	100 µm	200 µm	400 µm	800 µm
870°C-3h	0.07 (+ 0.18 T)	**0.04** (+ 0.10 T)	0.02 (+ 0.05 T)	0.00 (0 T)
920°C-3h	**0.14** (+ 0.36 T)	0.10 (+ 0.26 T)	**0.05** (+ 0.13 T)	0.01 (0 T)
920°C-12h	0.24 (+ 0.62 T)	0.19 (+ 0.49 T)	0.12 (+ 0.31 T)	0.05 (+ 0.13T)

Table 1: Dy/Nd_{init} ratio averaged over a 1-µm-thick grain shell of Dy diffused magnets, as estimated with the Fisher model (bold values correspond to the SEM/X-EDS pictures reported in Fig. 2). The values between brackets correspond to the estimated values of coercivity increase due to local Dy enrichment.

Three groups have been identified among the 12 cases considered and correspondingly color-coded: A (red) high concentration shells ($Dy/Nd_{init} > 0.12$), B (blue) intermediate concentration shells ($0.04 < Dy/Nd_{init} < 0.12$) and C (white) low concentration shells ($Dy/Nd_{init} < 0.04$).

Dy and Nd X-EDS elemental maps were acquired by SEM on the different samples and semi-quantitative concentration profiles have been extracted along lines of few microns length crossing the grain shells. Fig. 2 compares the Dy/Nd_{init} profiles given by SEM/X-EDS to the depletion calculated with the Fisher model for the magnets annealed at 870°C and 920°C (3h), at some characteristic depth values. For 920°C, two cases have been selected: (i) the grain concentration profile near the sample surface (100 µm, Fig. 2a) and (ii) the profile at a depth of 400 µm, corresponding to the intermediate average Dy content ($Dy/Nd_{init} \approx 0.05$, Fig. 2b). For 870°C, a profile is plotted for a depth of 200 µm where the Dy enrichment also lies within the intermediate range (Fig. 2c). It is worth noting that for the lowest Dy content regions (C), SEM/X-EDS semi-quantitative analyses are not accurate enough to correctly determine the Dy profile.

At 920°C-3h, the SEM/X-EDS profile in grains located near the surface exhibits a large plateau followed by a rapid decrease in the Dy content (Fig. 2a). This profile shape differs strongly from the calculated depletion line and reveals a different mechanism for the Dy penetration into the grain, as already pointed out by several authors. Near the sample surface, as the Dy concentration is high, a large amount of Nd is rejected to the GB phase and forms a thick liquid phase as the eutectic reaction proceeds. During cooling, the liquid phase solidifies and tends to transform into large and stepped shells with quasi-homogeneous Dy content [18].

The discrepancy tends to decrease for lower Dy contents, *i.e.* in the intermediate enrichment range (B). The agreement between the Fisher model and the SEM/X-EDS profiles is quite good, as illustrated by Fig.2b and 2c. The estimated values of local grain coercivity increment are also reported in Table 1 (values between brackets) for zones located up to 800 µm beneath the surface. For deeper zones, the coercivity increment is evaluated in accordance with the evolution in Dy enrichment calculated at a distance of 10 nm from the GB (Fig. 3). For instance, after annealing at 920°C-3h, the threshold for coercivity enhancement (Dy/Nd_{init} = 0.01) is located at 1.2 mm beneath the surface, meaning that the core region below this limit is assumed to be non-affected by the Dy diffusion annealing and maintains the properties of the base magnet.

3.2 Demagnetization curves

Experimental J-H curves measured on the same magnet, after successively removing layers from the top and bottom surfaces of the magnet, are plotted in Fig.4. Only the magnet annealed at 920°C-12h is shown, but the magnets annealed under other conditions showed identical trends. The inset of Fig. 4 shows J-H curves obtained on the reference magnet, before and after removal of a layer of 250 µm from the top and bottom surface of the magnet by polishing. This comparison serves to show that the evolution in the J-H curves obtained on the diffused samples can be attributed to the removal of high Dy-rich layers, rather than surface damage induced by polishing. Two 'knee' values of the magnetic field (H_{k1} and H_{k2}) are identified. It has been found that the diffusion annealing step didn't lead to an evolution of the first value H_{k1}, whatever the thickness of the removed layer, while the second, H_{k2}, is shifted towards higher values after diffusion annealing. A recoil curve was recorded after GBDP without polishing (Fig. 5) which clearly shows that irreversible demagnetization occurred in the sample for applied field values between H_{k1} and H_{k2}. However, residual magnetization mapping above the top surface of the magnet performed with a Hall probe indicates that no reversal had occurred in the top layer of the magnet, and the decrease in remanence after recoil is therefore attributed to partial reversal in the core of the magnet.

Fig.6 reports the decrease in the coercive field as a function of thickness of the removed layer for both samples annealed at 920°C (3 and 12h). It is worth noting that, in both cases, the largest decreases in H_c occurred when the external layers containing grains with thick shells of high Dy enrichment (zone A in section 3.1) were fully removed.

According to the previous Dy diffusion profiles and coercivity gradient evaluation, several 3D arrays of cubic grains (20×20×10, see Fig. 7) with the grain coercivity distribution parameters given in Table 2 have been simulated using the magnetostatic polycrystalline FE model. In the non-diffused regions of magnets, the mean grain switching field has been taken as $<\mu_0 H_c>$ = 1.6 T and the standard deviation equal to 0.2 T. The last value accounts for the shape of the J-H curve as measured on the reference magnet (see Fig. 8). For the other regions of magnets, which are affected by the Dy diffusion, the standard deviation has been assumed to be lower, i.e. σ_{Hc}= 0.1 T, assuming that Dy enrichment is more effcient for improving the coercivity of the weakest grains. However, this last assumption had few impact on the final results.

In the case of an annealing at 920°C-3h, the influence of the removal of external layers by polishing on the demagnetizing curve was also considered in the simulation. Complementary calculations where the upper zones (2, 3 and 4) were successively removed from the model were performed.

Zone index (nb of 2D arrays of cubic grains in the stack)	**Grain coercivity distribution parameters 920°C-3h**	**Grain coercivity distribution parameters 920°C-12h**	**Grain coercivity distribution parameters 870°C-3h**
Non-diffused central part zone #1 (4)	$<\mu_0 H_c>$ = 1.6 T - σ_{Hc}= 0.2 T	$<\mu_0 H_c>$ = 1.6 T - σ_{Hc}= 0.2 T	$<\mu_0 H_c>$ = 1.6 T - σ_{Hc}= 0.2 T
Low Dy-diffused zone #2 (2)	$<\mu_0 H_c>$ = 2.0 T - σ_{Hc}= 0.1 T	$<\mu_0 H_c>$ = 2.2 T - σ_{Hc}= 0.1 T	$<\mu_0 H_c>$ = 1.6 T - σ_{Hc}= 0.1 T
Medium Dy-diffused zone #3 (2)	$<\mu_0 H_c>$ = 2.2 T - σ_{Hc}= 0.1 T	$<\mu_0 H_c>$ = 2.4 T - σ_{Hc}= 0.1 T	$<\mu_0 H_c>$ = 2.0 T - σ_{Hc}= 0.1 T
High Dy-diffused zone #4 (2)	$<\mu_0 H_c>$ = 2.4 T - σ_{Hc}= 0.1 T	$<\mu_0 H_c>$ = 2.6 T - σ_{Hc}= 0.1 T	$<\mu_0 H_c>$ = 2.2 T - σ_{Hc}= 0.1 T

Table 2: Polycrystalline model configurations for simulated magnetization reversal in Dy-diffused samples corresponding to the three experimental diffusion conditions studied here.

Fig. 8 shows the evolution of the J-H curves simulated in the case of diffusion at 920°C-3h for four different stacks corresponding to the same sample but after successive layer removal by polishing (stack #1 = core zone to stack #4 = non-polished diffused magnet). It can be noticed that the J-H curves are highly stepped because of the relatively small

number of grains used in the model. More striking is the fact that the steps (*i.e.* the sudden drops in the polarization curve followed by a plateau), already observed during the demagnetization of the first stack (central zone), seem to translate to other J-H curves with an enlargement of the step width. This result reveals that grain reversal, once initiated in the central part, tends to extend upwards to the higher coercive layers. Grain reversal in the low coercive region is however triggered with a "delay" (i.e. the first reversal occurs for higher fields) compared to the situation occurring in the non-diffused magnet.

This situation is emphasized by the evolution of the grain reversal pattern simulated for the whole magnet (stack #4). Four points (A-D) are selected on the J-H curve (see Fig. 8) to highlight some important stages in the demagnetization process of the graded sample. The first grains that reverse at point A are the lowest coercivity grains located in the central zone. Until point B, grain switching happens mainly in this layer with a delay effect due to the magnetostatic "shielding" of the upper layers. After this "pivot" point B, reversal propagates easily towards the extremes of the magnet (point C) and coercivity (point D) is obtained at a field, H_c = 1340 kA/m (1.7 T). This value is much lower than what would be expected assuming that the external skin layer (zone 4 in Table 2) perfectly shielded the diffused magnet, *i.e.* H_c = 1910 kA/m (2.4 T), and is also lower than the average value obtained by weighing the contribution of each zone, *i.e.* H_c = 1590 kA/m (2.0 T).

4. Discussion

In this work, GBDP performed with a Dy-Co intermetallic alloy on sintered Nd-Fe-B magnets has been found to improve the switching field of hard grains over only 1-2 mm. This limitation comes from the consumption of the heavy rare-earth elements by the volume of grains located beneath the surface, as the HREE penetrates into the bulk of the magnet. The change in the diffusion annealing conditions tested here had a limited impact on the magnetic performance, as indicated in Fig. 9. Near the coercivity values, the J-H curves for 920°C-3h and 12h are found to be close, exhibiting quasi-superposition from point B (identified on figure 8 and corresponding to loss of shielding effect). The field off-set between the simulated J-H curves (≈60 kA/m) is greater than for the experimental curves (see dotted lines in Fig. 9.). This can be explained by the fact that the simulation poorly takes into account the complete depletion of Dy close to the surface of the magnet. Actually, with the Fisher model, one can estimate that all the available Dy deposited on

the surface should penetrate the sample after only 5h of diffusion treatment at 920°C. This limitation could explain why the experimental J-H curves for the 920°C-3h and 920°C-12h cases are very close. Moreover, at 920°C-3h more than 75 % of the available Dy atoms are estimated to diffuse up to 800-µm and are mainly 'consumed' by the grains (see thick shells in grains within 200µm of the original surface). This ratio increases to a value close to 100% when the diffusion time is increased to 12h, leading to thick shells in grains within 400 µm of the original surface. This evolution in the microstructure did not improve coercivity because the core of the magnet, poorly affected by diffusion and retaining low coercivity, had a strong demagnetization effect on the upper layers.

The simulated J-H curve for 870°C-3h is, as expected, shifted towards lower field values and the off-set compared to the magnet annealed at 920°C ($\Delta H \approx 100$ kA/m) is consistent with the experimental results ($\Delta H \approx 70$ kA/m). The reduction of the diffusion temperature by 50°C decreases the penetration depth and longer diffusion times are required to complete the thermal treatment. Finally, it can be stated that the optimal diffusion temperature for this alloy is around 900-920°C, confirming the previous study of Loewe [15] performed with different precursor alloys.

The ideal case for Dy diffusion would be achieved with deep penetration of the diffusing species along GBs, combined with a low consumption of Dy by grains, so that Dy would remain localized in thin shells of thickness 10 to 100 nm, at the grain rim. This would ensure that low additions of Dy (0.8 % wt.) would be efficient for coercivity enhancement, even for thick magnets. Examination of [Eq. 1] indicates that this optimal case corresponds to large values of the factor β. Restricting lateral diffusion inside grains to the GB thickness (a = 10 nm), requires fulfilment of the following condition: $\sqrt{D_v t} \approx a$. Then, the Dy concentration near GBs would be more homogeneous over large depths (d>1 mm) if the argument of the exponential term of [Eq. 1] remained lower than 1, *i.e.* if the ratio of the diffusion coefficients satisfied: $D_j/D_v > [d/a]^2$. With the selected target, this ratio should be $D_j/D_v > 10^{10}$. The values of D_j and D_v considered in the Fisher model, and consistent with the experimental results, lead to a ratio three orders of magnitude lower than the ideal value, explaining the limited efficiency of GBDP applied to thick magnets.

5. Conclusions

A heterogeneous distribution of Dy in the microstructure of thick sintered magnets after GBDP seems unavoidable, considering the diffusion mechanism involved. The magnetic

property gradient that results has a non-trivial impact on the resistance to demagnetization of the magnet, which depends also on the external magnetic circuit. The polycrystalline model provides a better understanding of the grain reversal sequence in graded magnets tested in closed-circuit. In this configuration, demagnetization starts from the less coercive grains located at the core of the magnet, remains constricted in this zone thanks to a shielding effect from the external surface, but then propagates towards outer layers via magnetostatic interactions. When the coercivity gradient is large, as in the 5-mm-thick magnets studied in this work, the coercivity of the whole magnet, measured in closed-circuit, could be 100-200 kA/m lower than the value expected without considering magnetostatic interactions, *i.e.* after averaging the coercive field of each zone. This result suggests that the shielding effect from the diffusion affected layers could be limited and counterbalanced by magnetostatic interactions. Specific dimensioning could be required when using thick Dy-diffused magnets in electrical devices [19], especially when closed-circuit configurations prevail.

References

[1] H. Sepehri-Amin, S. Hirosawa, and K. Hono, "Advances in Nd-Fe-B Based Permanent Magnets," in *Handbook of Magnetic Materials*, vol. 27, Elsevier, 2018, pp. 269–372.

[2] K. T. Park and M. Sagawa, "Effect of metal-coating and consecutive heat treatment on coercivity of thin Nd-Fe-B sintered magnets," *16th Int Workshop Rare-Earth Magn. Their Appl.*, 2000.

[3] K. Löewe, C. Brombacher, M. Katter, and O. Gutfleisch, "Temperature-dependent Dy diffusion processes in Nd–Fe–B permanent magnets," *Acta Mater.*, vol. 83, pp. 248–255, Jan. 2015.

[4] F. Vial, F. Joly, E. Nevalainen, M. Sagawa, K. Hiraga, and K. T. Park, "Improvement of coercivity of sintered NdFeB permanent magnets by heat treatment," *J. Magn. Magn. Mater.*, vol. 242, pp. 1329–1334, 2002.

[5] M. Soderžnik *et al.*, "Magnetization reversal of exchange-coupled and exchange-decoupled Nd-Fe-B magnets observed by magneto-optical Kerr effect microscopy", *Acta Mater.*, vol. 135, pp. 68–76, Aug. 2017.

[6] J. Fliegans, G. Delette, A. N. Dobrynin, N. M. Dempsey, and D. Givord, "Closed-Circuit Versus Open-Circuit Characterization of Hard Magnets," *IEEE Trans. Magn.*, vol. 55, no. 2, pp. 1–5, Feb. 2019.

[7] J. Fliegans, O. Tosoni, N. M. Dempsey, and G. Delette. "Modeling of demagnetization processes in permanent magnets measured in closed-circuit geometry", *Appl. Phys. Lett.* 116, 062405 (2020)

[8] T. Schrefl, H. F. Schmidts, J. Fidler, and H. Kronmuller, "Nucleation fields and grain boundaries in hard magnetic materials," *IEEE Trans. Magn.*, vol. 29, no. 6, pp. 2878–2880, 1993.

[9] J. C. Fisher, "Calculation of Diffusion Penetration Curves for Surface and Grain Boundary Diffusion," *J. Appl. Phys.*, vol. 22, no. 1, pp. 74–77, 1951.

[10] R. T. P. Whipple, "CXXXVIII. Concentration contours in grain boundary diffusion," *Lond. Edinb. Dublin Philos. Mag. J. Sci.*, vol. 45, no. 371, pp. 1225–1236, 1954.

[11] T. Suzuoka, "Exact Solutions of Two Ideal Cases in Grain Boundary Diffusion Problem and the Application to Sectioning Method," *J. Phys. Soc. Jpn.*, vol. 19, no. 6, pp. 839–851, 1964.

[12] M. Sagawa, S. Fujimura, H. Yamamoto, Y. Matsuura, and K. Hiraga, "Permanent magnet materials based on the rare earth-iron-boron tetragonal compounds," *IEEE Trans. Magn.*, vol. 20, no. 5, pp. 1584–1589, Sep. 1984.

[13] B. B. Straumal et al., "Grain boundary phenomena in NdFeB-based hard magnetic alloys," *Rev. Adv. Mater. Sci*., vol. 38, no. 1, 2014.

[14] M. F. De Campos and J. A. De Castro, "Optimizing the Heat Treatment of Rare Earth-Transition Metal Sintered Magnets," in *Materials Science Forum*, 2010, vol. 660, pp. 290–295.

[15] K. Loewe, D. Benke, C. Kübel, T. Lienig, K. P. Skokov, and O. Gutfleisch, "Grain boundary diffusion of different rare earth elements in Nd-Fe-B sintered magnets by experiment and FEM simulation," *Acta Mater.*, vol. 124, pp. 421–429, Feb. 2017.

[16] H. Sepehri-Amin, T. Ohkubo, and K. Hono, "Grain boundary structure and chemistry of Dy-diffusion processed Nd–Fe–B sintered magnets," *J. Appl. Phys.*, vol. 107, no. 9, p. 09A745, May 2010.

[17] T.-H. Kim *et al.*, "Microstructure and coercivity of grain boundary diffusion processed Dy-free and Dy-containing Nd Fe B sintered magnets," *Acta Mater.*, vol. 172, pp. 139–149, Jun. 2019.

[18] N. Oono, M. Sagawa, R. Kasada, H. Matsui, and A. Kimura, "Production of thick high-performance sintered neodymium magnets by grain boundary diffusion treatment with dysprosium–nickel–aluminum alloy," *J. Magn. Magn. Mater.*, vol. 323, no. 3–4, pp. 297–300, Feb. 2011.

[19] M. P. Thompson *et al.*, "Grain-Boundary-Diffused Magnets: The challenges in obtaining reliable and representative BH curves for electromagnetic motor design," *IEEE Electrification Mag.*, vol. 5, no. 1, pp. 19–27, Mar. 2017.

Figure captions

Figure 1: 3D geometrical model used for the simulation in closed-circuit configuration (hysteresigraph measurement system: 1=magnet, 2=pole pieces, 3=yoke, 4=coil winding, 5=flux sensor).

Figure 2: Nd and Dy elemental maps (right) and Dy/Nd_{init} profiles (left) obtained by SEM/X-EDS analysis for three selected depths and annealing conditions. Dy/Nd_{init} values (open red symbols) are determined along the half red lines crossing GBs, indicated on the SEM images, and are compared to calculated profiles obtained with the Fisher model (solid lines).

Figure 3: Evolution of the Dy enrichment at 10 nm from the grain boundary, as a function of the distance from the sample surface, calculated using the Fisher model for the three diffusion conditions studied here.

Figure 4: Experimental demagnetization curves after Dy diffusion annealing (920°C-12h) obtained on the same magnet before and after removal of layers from the top and bottom surfaces of the magnet by polishing (the layer thickness removed during the successive polishing steps is given in the legend). J-H curves of the reference magnet before and after removal of a layer from the top and bottom surfaces of the magnet by polishing is plotted in the inset figure.

Figure 5: Residual induction maps above the top of a Dy-diffused sample (920°C-3h) at three remanent states (1-after saturation, 2-partial demagnetization after the recoil curve discussed in the text, 3-coercivity state), measured using a scanning Hall probe. $B_{z,moy}$ denotes the average value of the residual induction measured in the scanned plane (400 µm above the magnet).

Figure 6: Evolution of the sample coercive field as a function of the thickness of the layer removed from the top and bottom surfaces of the magnet by polishing, the coercive field is normalized with respect to the value obtained on the non-polished magnet. Inset figures correspond to Dy X-EDS element maps acquired by SEM at selected depths.

Figure 7: Cross-section in the middle (XZ) plane of the complete 3D-array of cubic grains with four zones accounting for the coercivity gradient. The grains are colored in a gray scale according to their switching field value (black=lowest value, white=highest value) ascribed according to a Gaussian distribution with parameter values indicated in Table 2 (symmetrical parts duplicated).

Figure 8: Demagnetization curves simulated with magnetic properties given in Table 2 for the sample annealed at 920°C-3h (stack #1= zone 1, stack #2= zones 1+2, stack #3= zones 1+2+3, stack #4= zones 1+2+3+4). The grain reversal patterns in the median (XZ) plane (gray=reversed, white non-reversed) at selected points (A-D) of the J-H curve are also given.

Figure 9: Experimental and simulated demagnetization curves obtained with the input data reported in Table 2 on the entire magnet (without polishing) for the three conditions of diffusion annealing studied here.

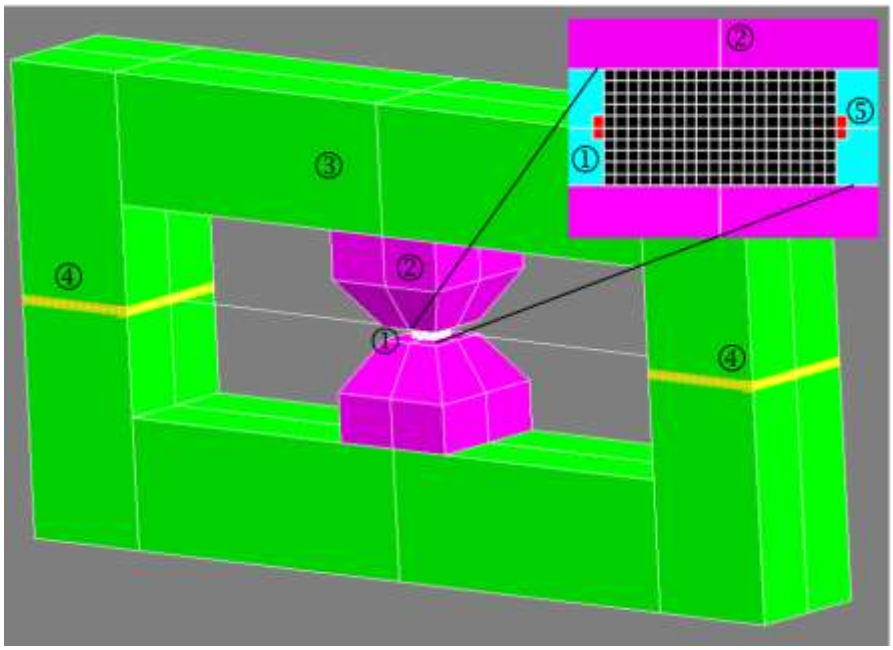

Figure 1: 3D geometrical model used for the simulation in closed-circuit configuration (hysteresigraph measurement system: 1=magnet, 2=pole pieces, 3=yoke, 4=coil winding, 5=flux sensor).

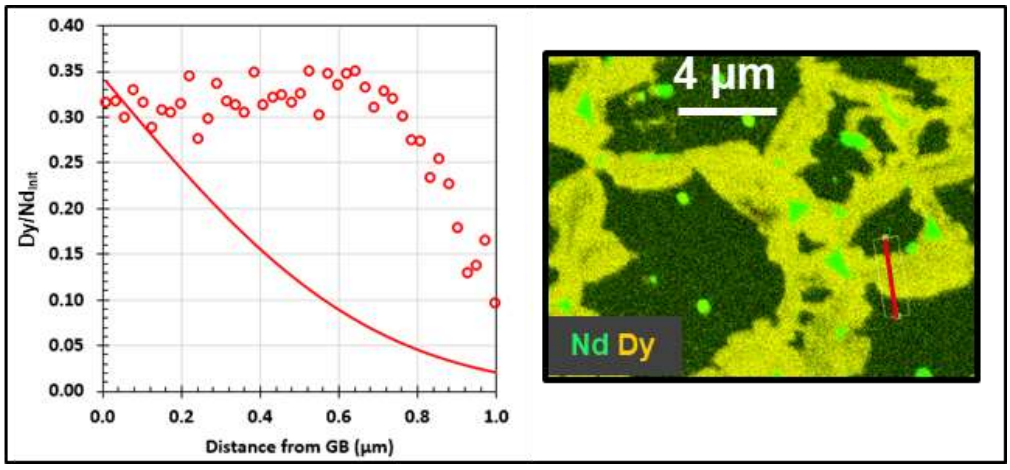

a) 920°C-3h-100 µm

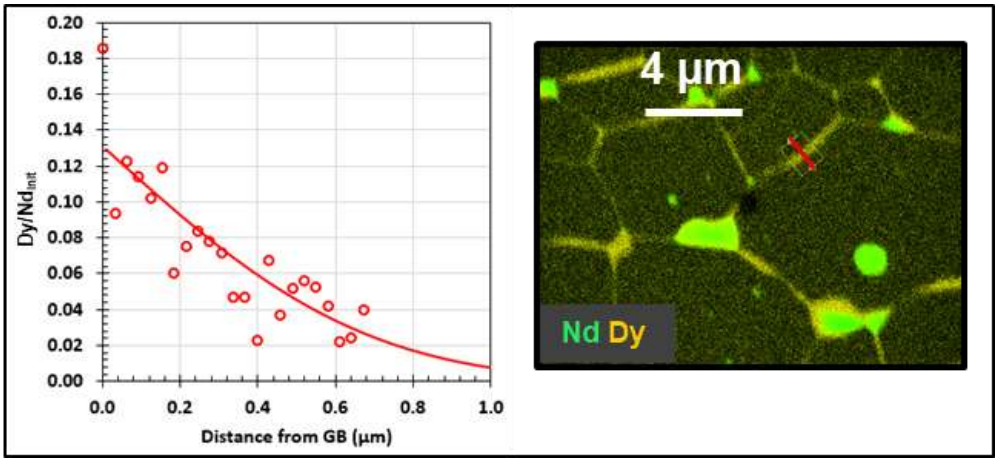

b) 920°C-3h-400 µm

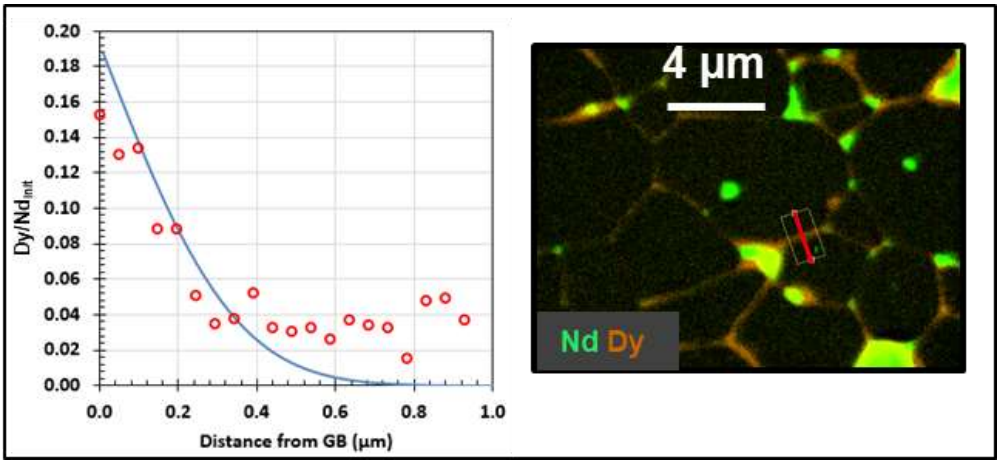

c) 870°C-3h-200 µm

Figure 2: Nd and Dy elemental maps (right) and Dy/Nd_{init} profiles (left) obtained by SEM/X-EDS analysis for three selected depths and annealing conditions. Dy/Nd_{init} values (open red symbols) are determined along the half red lines crossing GBs, indicated on the SEM images, and are compared to calculated profiles obtained with the Fisher model (solid lines).

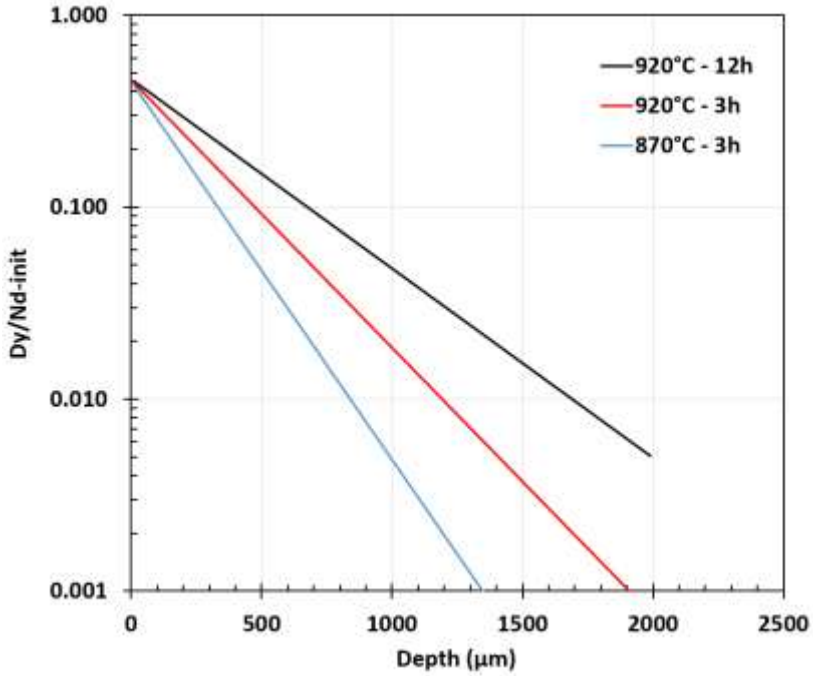

Figure 3: Evolution of the Dy enrichment at 10 nm from the grain boundary, as a function of the distance from the sample surface, calculated using the Fisher model for the three diffusion conditions studied here.

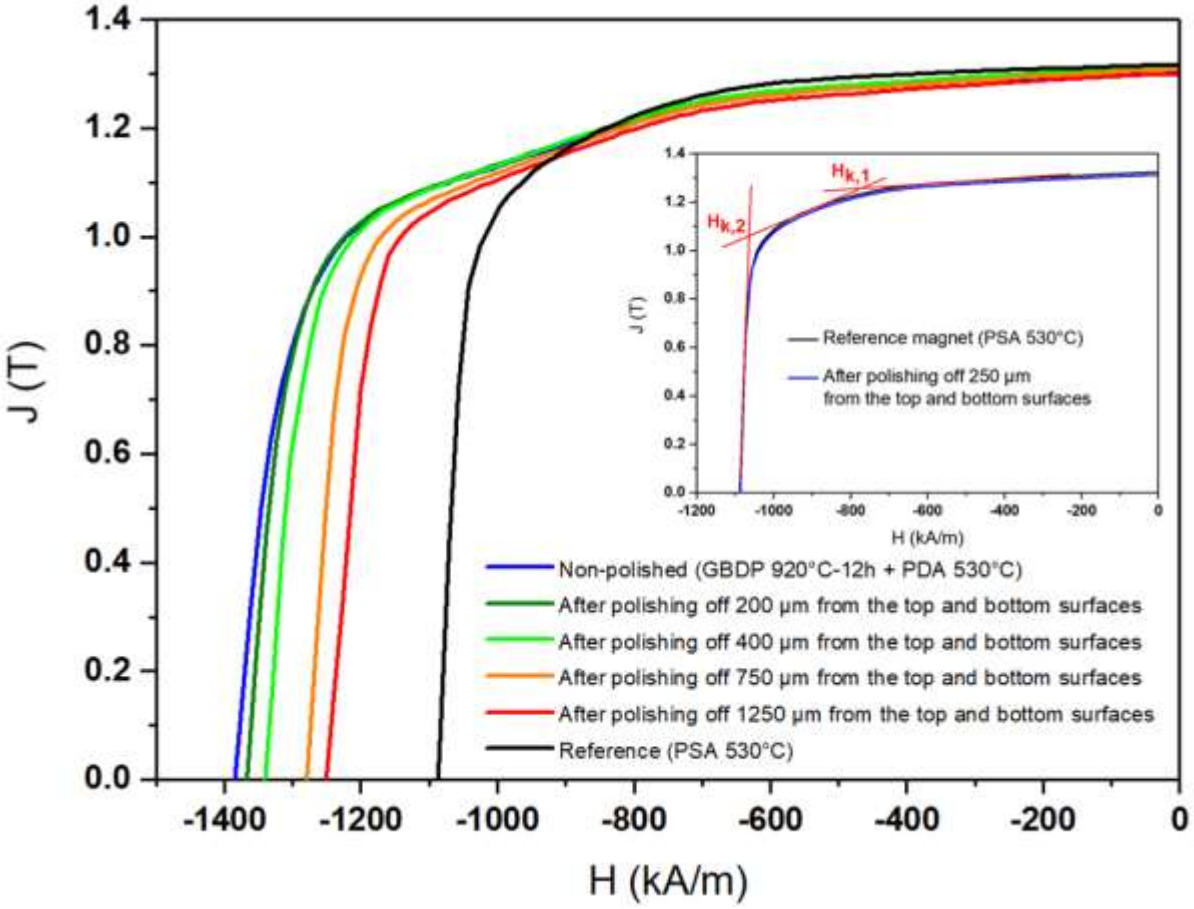

Figure 4: Experimental demagnetization curves after Dy diffusion annealing (920°C-12h) obtained on the same magnet before and after removal of layers from the top and bottom surfaces of the magnet by polishing (the layer thickness removed during the successive polishing steps is given in the legend). J-H curves of the reference magnet before and after removal of a layer from the top and bottom surfaces of the magnet by polishing is plotted in the inset figure.

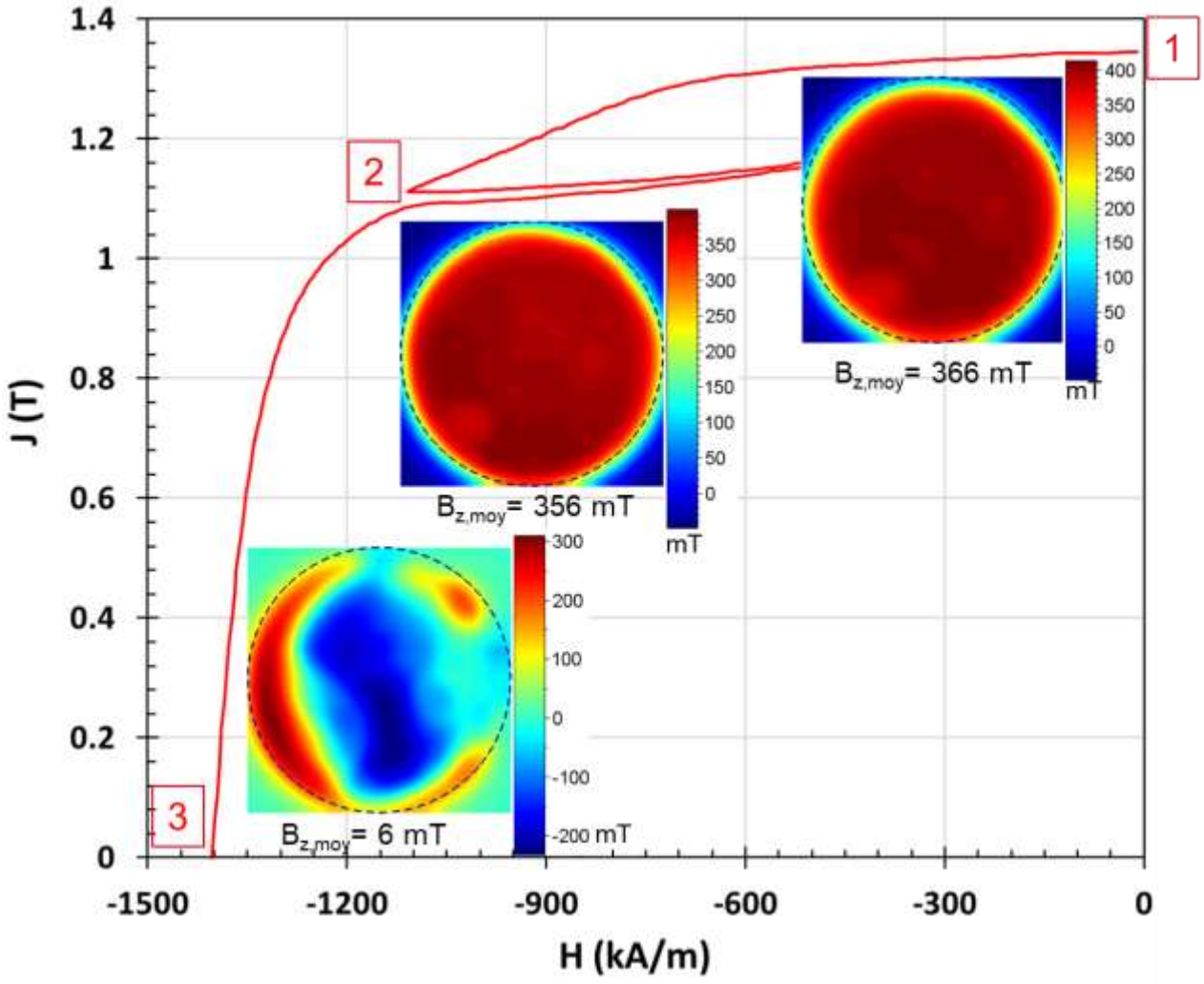

Figure 5: Residual induction maps above the top of a Dy-diffused sample (920°C-3h) at three remanent states (1-after saturation, 2-partial demagnetization after the recoil curve discussed in the text, 3-coercivity state), measured using a scanning Hall probe. $B_{z,moy}$ denotes the average value of the residual induction measured in the scanned plane (400 µm above the magnet).

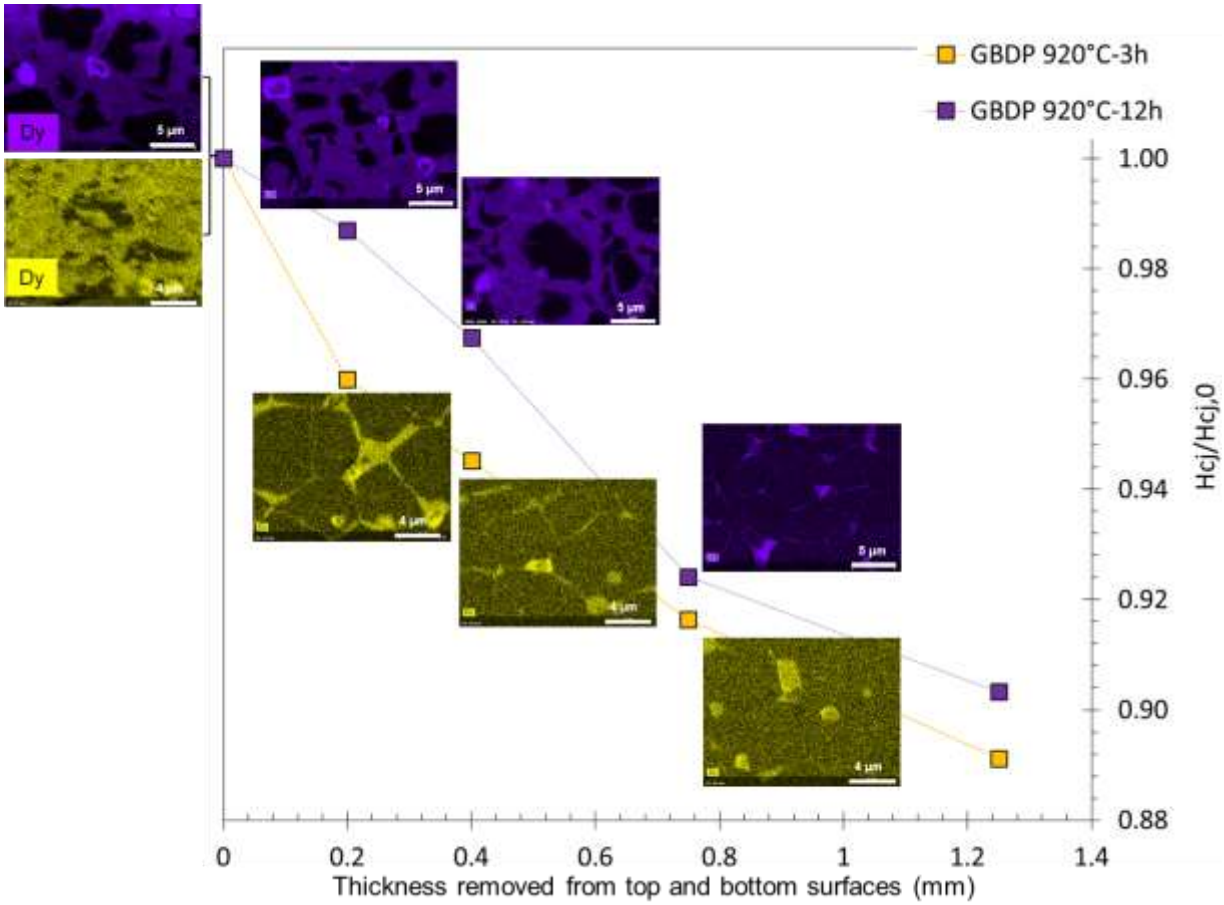

Figure 6: Evolution of the sample coercive field as a function of the thickness of the layer removed from the top and bottom surfaces of the magnet by polishing, the coercive field is normalized with respect to the value obtained on the non-polished magnet. Inset figures correspond to Dy X-EDS element maps acquired by SEM at selected depths.

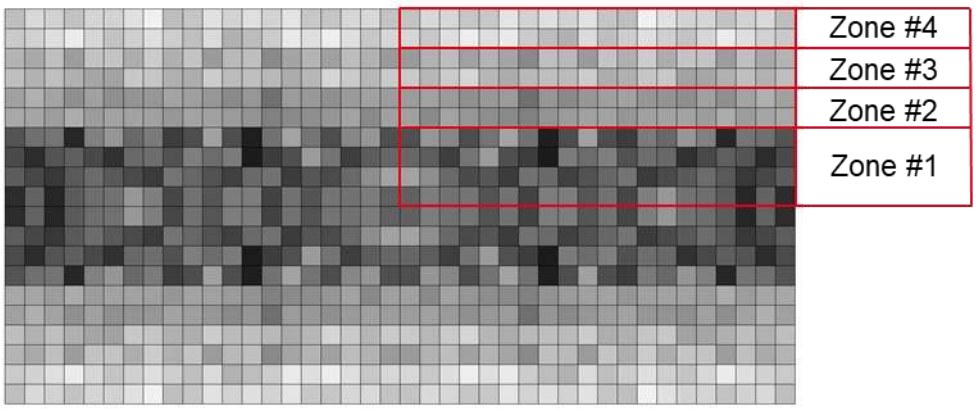

Figure 7: Cross-section in the middle (XZ) plane of the complete 3D-array of cubic grains with four zones accounting for the coercivity gradient. The grains are colored in a gray scale according to their switching field value (black=lowest value, white=highest value) ascribed according to a Gaussian distribution with parameter values indicated in Table 2 (symmetrical parts duplicated).

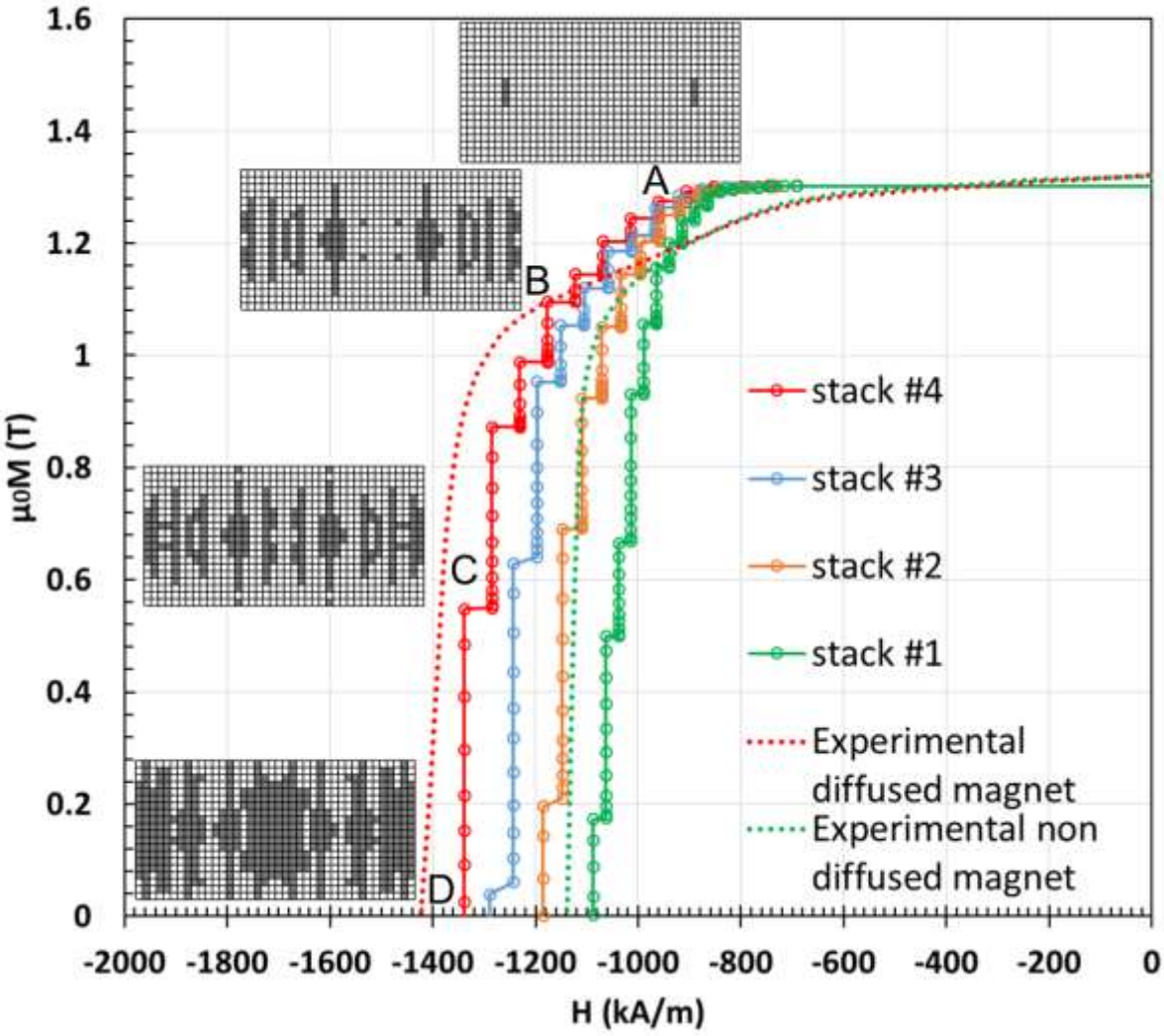

Figure 8: Demagnetization curves simulated with magnetic properties given in Table 2 for the sample annealed at 920°C-3h (stack #1= zone 1, stack #2= zones 1+2, stack #3= zones 1+2+3, stack #4= zones 1+2+3+4). The grain reversal patterns in the median (XZ) plane (gray=reversed, white non-reversed) at selected points (A-D) of the J-H curve are also given.

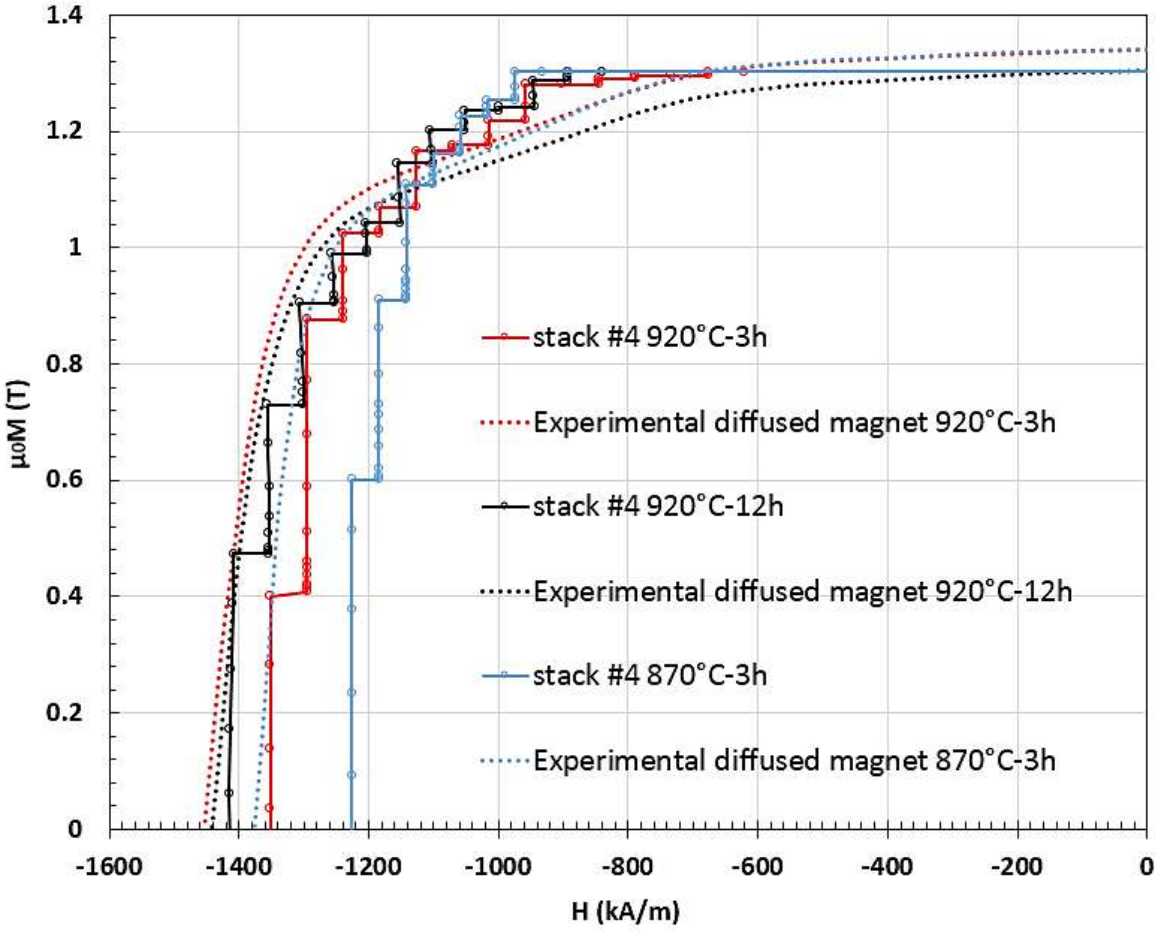

Figure 9: Experimental and simulated demagnetization curves obtained with the input data reported in Table 2 on the entire magnet (without polishing) for the three conditions of diffusion annealing studied here.